

P-WAE: Generalized Patch-Wasserstein Autoencoder for Anomaly Screening

Hui Zhang, *Member IEEE*, Yurong Chen, *Member IEEE*, Yaonan Wang, Yihong Cao, Q. M. Jonathan Wu, *Senior Member IEEE*, Yimin Yang, *Senior Member IEEE*

Abstract—To mitigate the inspector’s workload and improve the quality of the product, computer vision-based anomaly detection (AD) techniques are gradually deployed in real-world industrial scenarios. Recent anomaly analysis benchmarks progress to generative models. The aim is to model the defect-free distribution so that anomalies can be classified as out-of-distribution samples. Nevertheless, there are two disturbing factors that need researchers and deployers to prioritize: (i) the simplistic prior latent distribution inducing limited expressive capability; (ii) the collapsed mutual-dependent features resulting in poor generalization. In this paper, we propose a novel Patch-wise Wasserstein AutoEncoder (P-WAE) architecture to alleviate those challenges. In particular, a patch-wise variational inference model coupled with solving the *jigsaw* puzzle is designed, which is a simple yet effective way to increase the expressiveness and complexity of the latent manifold. This alleviates the blurry reconstruction problem. In addition, the Hilbert-Schmidt Independence Criterion (HSIC) bottleneck is introduced to constrain the over-regularization representation. Comprehensive experiments, conducted on the MVTec AD dataset, demonstrate the superior performance of our proposed method.

Index Terms—Anomaly Detection, Variational Inference, Representation Learning, Patch Distribution Modelling.

I. INTRODUCTION

Naturally recognizing anomaly (or threat) is one of the prominent characteristics of human intelligence. Whenever we watch animals, we recognize what they are and evaluate whether they could be a threat, simultaneously [1]. This novelty perception capability is desired for modern machine learning algorithms. Therefore, a significant amount of research interest has been directed towards outlier detection that would like to mimic this intelligence. Anomaly detection (AD) denotes identifying the observations that are non-conforming to the normal patterns. It is quite relevant in many

application fields, such as industrial optical inspection [2], medical imaging analysis [3], and video surveillance [4].

Starting from the first statistics community study for anomaly detection as early as the 19th century [5][6], over time, a spectrum of anomaly detection methods have been proposed. One of the research fields focuses on the direct classification of the inlier and outlier [7][8][9]. These models learn the discriminative outlier distribution, then utilize the logistic function to separate anomalies in a hyperplane. While they yield satisfying results in a particular case, the expert annotated signal deters their deployment in real-world scenarios. In addition, the skewed distribution (an unlimited supply of the normal data, but abnormalities) makes network learning worse [35]. On the other hand, the One-Class Classification (OCC)-based technique for AD is widely adopted because it casts off the demand for the anomaly data [11].

The core of OCC is to learn a model that fits the characteristics of “normality.” Deviations from this description are then deemed to be outliers. The prerequisite for the successes of previous works such as the One-Class SVM [12] and Deep SVDD [11], is the availability of corpora normal data. Otherwise, the decision boundary is sensitive, unstable, and hard to bound, especially dealing with complex, high-dimensional data. To address this shortcoming, the generative-based OCC algorithm attracts the interest of researchers. Different with directly learning the representation embedding space of normal data, generative methods explicitly [13] or implicitly [14] model the true normal data distribution.

Variational autoencoder (VAE) [13] is one of the most prevailing generative methods for anomaly detection [15][16][17]. Rooted in Bayesian inference, the network transforms the modelling arbitrary data space into the latent space while remaining the data manifold structure. Based on the *analysis-synthesis* idea, the parameterized *inference* and *generative* network of VAE are trained jointly via maximizing the evidence lower bound (ELBO) [13][19]. This is equivalent to minimizing the divergence between the prior and inference posterior distribution. With only training on the defect-free data, the learned latent distribution can be viewed as the normal manifold. One feasible solution to threshold the anomaly is to generate the input data per-pixel depending on the latent features, where the normal data can be reconstructed well but the anomaly [15][16][17][18]. Despite their state-of-the-art performance [2], unsupervised VAE-based abnormality screening is still ill-posed. In particular, this paper investigates the two primary challenges that need researchers to prioritize.

Firstly, VAE [13] is theoretically elegant and easy to

This work is supported in part by the National Natural Science Foundation of China under Grant 61971071, Grant 62027810, and Grant 61701047, 61733004, in part by the National Key R&D Program of China under Grant 2018YFB1308200, in part by the Hunan Key Project of Research and Development Plan under Grant 2018GK2022.

H. Zhang, Y. Chen, Y. Wang, and Y. Cao are with the National Engineering Laboratory of Robot Visual Perception and Control Technology, School of Robotics, Hunan University, Changsha, Hunan, 410082 China (e-mail: zhanghuihy@126.com, chenyrong1998@outlook.com, yaonan@hnu.edu.cn, caoyihong97@foxmail.com). Corresponding author: Hui Zhang.

Q. M. J. Wu is with the Department of Electrical and Computer Engineering,, University of Windsor, Windsor, Ontario, N9B3P4 Canada (e-mail: jwu@uwindsor.ca).

Y. Yang is with the Department of Computer Science, Lakehead University, Ontario, P7B 5E1, Canada, also with the Vector Institute, Toronto, M5G 1M1, Canada. (e-mail: yyang48@lakeheadu.ca).

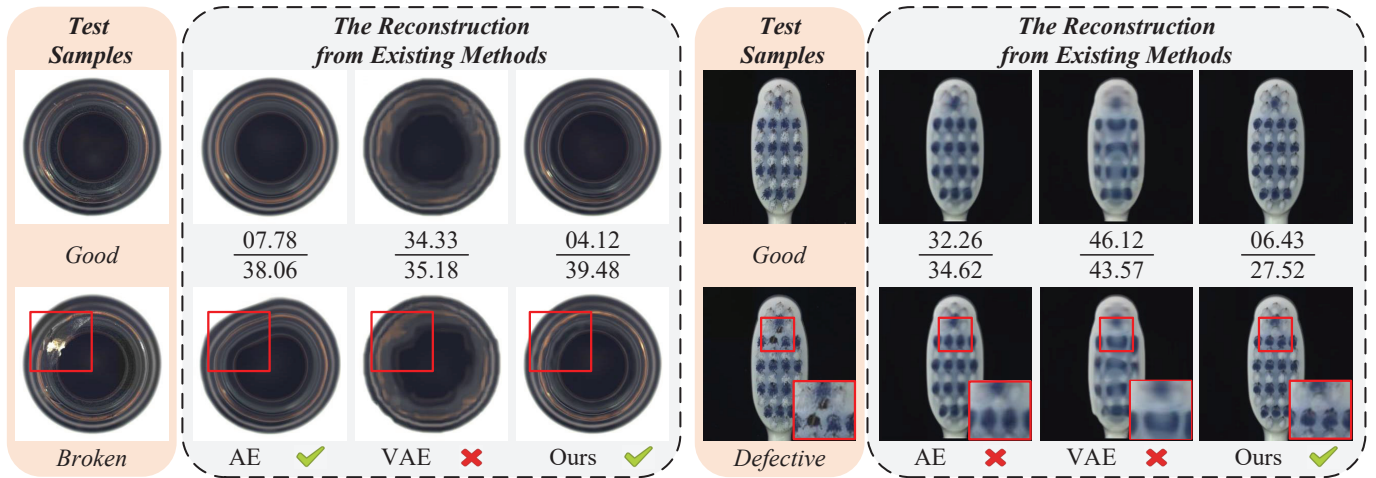


Fig. 1: We visualize the main problems of previous works. The middle row is the ratio of the good and anomaly reconstruction error. The vanilla autoencoder (AE) [29] shows that the reconstruction of the anomaly deviates from the normal patterns. And both the reconstruction of defect-free and anomaly from variational autoencoder (VAE)[13] shows over-smooth. Our proposed method can generate high-fidelity data to classify the outlier.

train. However, the generated images of VAE-based anomaly detection methods are observed vague, as they often only semantically resemble the inputs, not in pixel values [20], as Fig. 1 shows. Recent studies tend to attribute this negative phenomenon to the simplistic prior distribution (e.g. isotropic Gaussian) [21][22]. There are two main approaches to mitigate the problem. One can increase the complexity of the latent prior distribution, such as utilizing the Mixture of Gaussian (MoG) [21][22]. However, the optimization of the mixture model is not allowed with a closed-form in divergence computation so that they rely on the Markov chain Monte Carlo samples [21]. Although the sliced-Wasserstein empirically provides an alternative divergence for optimization [22], the performance is sensitive to the hyper-parameters of components of MoG and random projection. Another solution is to construct patches' distribution from the whole image and then inspect the defect on each patch [17][23][24]. These methods avoid treating the training image as a whole, however, omitting the simultaneous learning of local and global information. Meanwhile, the complex patch selection mechanism is difficult to be deployed in practical anomaly detection applications.

Secondly, the main objective of VAE-based AD is to disentangle then retain the meaningful representations of the normal data. In other words, the model is optimized to extract the non-trivial features that can maintain the input data manifold. As mentioned above, the latent variables are learned via fitting to the prior distribution [13], where the f -divergence is commonly used as the density measure. However, this strong notions of distances often max out, providing useless gradients thus inducing over-regularization and collapsed features [25], consequently, "well" approximation. Analyzing from the information theory perspective, merely minimizing the f -divergence encourages the mapped representation to carry less information about the input [26] (the theoretical verification about the relationship of divergence and information is provided in the Section 3.D). WAE and SWAE [25][22] alleviate this

issue by introducing a weaker topology probability measure (Wasserstein distance) from the optimal transport point of view. They strengthen the connection between the generative samples and the inputs via waiving the reparameterizing trick [13], however, there is no evidence that shows the true data distribution could be further encoded. Moreover, Information bottleneck (IB) [27] is the paradigm to balance the conditional entropy of latent variables given the inputs and outputs. Yet it has not been widely explored in VAE-based anomaly detection. One obstruction could be the practical difficulties of calculating the mutual information [28].

In this paper, motivated by the philosophy of autoencoders [29] [30] [31], we propose a novel Patch-wise Wasserstein AutoEncoder (P-WAE) architecture to address these two challenges in the area of anomaly detection. Firstly, due to the univariate Gaussian prior is unable to generate a whole high-fidelity image, we investigate whether can transform the approximating of the mixture priors distribution into multiple simple patch-wise priors. Motivated by previous patch-based modelling algorithms [17][23], we design an original patch-wise variational inference network to set up a more powerful latent manifold. One of the main improvements is that we take the shuffled image tiles as the input patches, then assign diverse prior distributions, individually. This is a generalized and effective way to construct patches. Coupled with solving the *jigsaw puzzle* [32] as the auxiliary task, the model can learn to capture global and local representations of normal data. Secondly, to deal with the collapsed features learned by the strong metric, we introduce a weaker distribution distance measure. In addition, we explore a non-parametric kernel-based norm, named Hilbert-Schmidt Independence Criterion (HSIC) in anomaly detection. The HSIC bottleneck can be used as the constraining of the uninformative representation. In conclusion, our contributions can be summarized as follows:

- We propose P-WAE architecture for anomaly detection. This is a simple yet effective method to remain a more

accurate manifold of normal data. With solving *jigsaw puzzle* as the auxiliary task, the latent codes can capture both global and local information, which encourages the network to generate high-resolution images.

- We introduce a sliced-Wasserstein measure and HSIC bottleneck to alleviate the collapsed features, which is negative for the network’s generalization capability. In addition, these are computationally less expensive in contrast with common divergence.
- The proposed method shows superior performance on anomaly detection, including but not limited to industrial defect detection.

II. RELATE WORK

A. Anomaly Detection

The anomaly detection methods focus on density estimation of normal data, which gets rid of the demand for outlier datasets. The early interests can be found in the statistical literature [5]. Statistical classifier theory thrives on the methodology of robust estimation on outlier detection [33]. Those traditional methods, such as, One-class SVM [12], SVDD [34], rely on hand-crafted features, however, suffer from *curse of dimensionality* when applied to high-dimensional complex data directly. Existing methods follow the paradigm of deep feature extraction and normal distribution learning. For example, Deep SVDD [11] fits the neural network outputs into a hypersphere of minimum volume. Perera et al. [35] introduce a compactness loss and descriptiveness loss to constrain the latent space. GeoTrans [36] and ITAE [37] rely on geometric transforms to learn the normal features. Deep autoencoders (AE) [29], trained to minimize the reconstruction error, are the predominant method used for learn the shared factors of variation from normal samples. A deep AE with a parametric density estimator is proposed by Davide [38] for novelty detection. Wang et al. propose structural similarity [39] which is beneficial for improving the convolutional autoencoder-based AD [40]. In addition, the anomaly detection based on generative adversarial networks (GANs) [3][41][42] can explicitly learn to fit normal data distribution. While GANs-based methods generally yield visually sharper image data, they are limited by no maneuverable latent space and unstable training.

B. Generative Model

Generative models in the context of the variational Bayes technique, have shown great promise in modelling complex distributions. Variational autoencoders (VAEs) [13] are theoretically elegant and easy to train. However, VAEs-based anomaly detection methods are observed that the reconstruction results often only vaguely resemble the input and often do so only semantically and not in terms of pixel values [20]. With these over-smooth reconstructed images, it is difficult to set a threshold to classify the outlier and inlier. InfoVAE [43] weighs the preference between correct inference and prior distribution and the reliance on the latent variables. (Sliced) Wasserstein distance is utilized in WAE [25], SWAE [22]

to replace the traditional divergence metrics. They encourage networks to generate high-resolution photo-realistic images and preserve true posterior simultaneously. However, it ignores that the approximate posterior distribution is often simplistic and different from the true posterior. Researchers made effort on utilizing Gaussian mixture mode. Moreover, CBiGAN [44] achieves superior results via discriminating jointly in the data and latent space. However, hybrid networks struggle to scale, evaluate and utilize for inference due to the use of classifier probabilities and still fall short in terms of diversity.

C. Information theory-based Method

The core of representation learning is to explore the relevant and significant features, which allows us to generate images [29] for anomaly detection. One neat idea is to train a function (i.e. an encoder) via maximizing the mutual information (MI) between its inputs and outputs [45]. The informax principle [46] is the bedrock of component analysis studies but is difficult to adapt for the deep neural network as we typically have access to data samples but the distributions [47]. Without estimation MI, numerous methods derive the bounds on MI [27][19]. Information bottleneck (IB) [27] proposed by Prof. Tishby et al., is optimized to constrain the entropy of latent features about inputs and outputs [19]. The techniques construct and maximize the MI in order to obtain meaningful representations is proposed in [48]. However, simply maximizing the MI encourages the latent representations to be redundant and prevents the disentanglement of local and global factors. This is often known as posterior collapse [49] that the expressive generative networks ignore the latent variables and inference networks. To mitigate this issue, β -VAE [49] regularizes the MI to prevent representations from becoming uninformative. Similar with the idea of IB [27], HSIC bottleneck [28] adopts a non-parametric kernel-based criterion to learn more robust representations.

III. METHOD

In this section, we first formulate the problem of anomaly detection in Section 3. A. Secondly, the related background knowledge about the variational inference and information theory will be revisited in Section 3. B. Furthermore, the patch-wise distribution modelling method is provided in Section 3. C. The HSIC bottleneck-based autoencoder objective is discussed in Section 3. D. Last but not least, the whole framework is provided in Section 3. E.

A. Problem Formulation

This work considers the anomaly screening under an unsupervised setting. Given a large training dataset D_X comprising N samples ($D_X = \{x_1, x_2, \dots, x_N\}$ where $x_i \in \mathcal{X}$ is an individual input data point sampled from defect-free manifold \mathcal{X} in Euclidean space), the core objective of anomaly detection is to model D_X and learn its manifold \mathcal{X} . Let \mathcal{Z} be the representation space, and $z_i \in \mathcal{Z}$ is the latent features of x_i . The realization of deep anomaly detection is to train a feature mapping function $f_\varphi(\cdot) : \mathcal{X} \rightarrow \mathcal{Z}$ and an outlier estimation

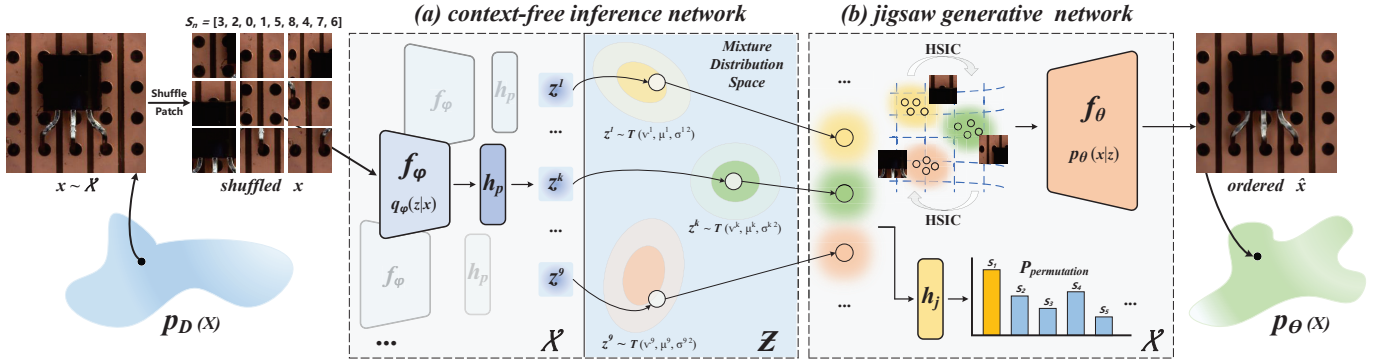


Fig. 2: Illustration of our proposed method architecture, which consists of two main modules. During the training phase, given x sampled from the normal data manifold \mathcal{X} , its puzzle obtained by shuffling the tiles via a randomly chosen permutation. Then they are fed to the (a) context-free inference network, which is the Siamese-wise encoder $f_\varphi(\cdot)$. It is to inference the mixture posterior distribution $\sum q(z^k|x^k)$. The approximated latent codes z are then sent to (b) jigsaw generative network. This decoder architecture aims to reconstruct the input and solve the *jigsaw puzzle*, simultaneously. In addition, the representation of the generated samples is regularized via the HSIC bottleneck objective.

function $f_\theta(\cdot) : \mathcal{Z} \rightarrow \mathcal{X}$. Based on the deep autoencoder philosophy [29], $f_\varphi(\cdot)$ and $f_\theta(\cdot)$ can be parameterized by two neural network, often known as the encoder and decoder. In this case, the $f_\varphi(\cdot)$ is utilized to generate a low-dimensional features that represents the normal distribution, and $f_\theta(\cdot)$ is required to reconstruct the original normal space with the latent codes. Anomalies recognition in the testing phase can be achieved by setting a threshold value ϵ of the L_n -reconstruction error:

$$\|x_i, \hat{x}_i\|_n = \|x_i, f_\theta(f_\varphi(x_i))\|_n \geq \epsilon \in \mathbb{R}. \quad (1)$$

B. Preliminary

Variational autoencoders. Similar to the classic autoencoder [29], VAEs [13] consists of two components: an inference network (encoder) $q_\varphi(z|x) \subseteq f_\varphi(\cdot)$ and a generative network (decoder) $p_\theta(x|z) \subseteq f_\theta(\cdot)$. It's not only approximated and recovered x from z but it estimates the true underlying distribution $p_D(x)$. The natural approach is maximum marginal log-likelihood $\log p_\theta(x)$:

$$\mathbb{E}_{p_D(x)}[\log p_\theta(x)] = \mathbb{E}_{p_D(x)}[\log \mathbb{E}_{p(z)}[p_\theta(x|z)]], \quad (2)$$

where $p_\theta(x)$ is the model distribution, and $p(z)$ denotes the distribution over the latent feature. However, it is intractable due to the integration operation of computing $p_\theta(x) = \int_z p_\theta(x|z)p(z)dz$. One common technique is introducing an amortized distribution, $q_\varphi(z|x)$, and optimizes the tractable Evidence Lower Bound (ELBO) to the log-likelihood:

$$\begin{aligned} \log p_\theta(x) &\geq \mathbb{E}_{q_\varphi(z|x)}[\log p_\theta(x, z) - \log q_\varphi(z|x)] \\ &= \mathbb{E}_{q_\varphi(z|x)}[\log p_\theta(x|z)] - D_{KL}(q_\varphi(z|x) \parallel p(z)) \\ &:= \mathcal{L}_{ELBO}(x; \theta, \varphi). \end{aligned} \quad (3)$$

It includes the expected conditional log-likelihood and the Kullback-Leibler (KL) divergence D_{KL} between the inference distribution and a prior distribution. Maximizing the likelihood equals maximizing the ELBO. If there is φ such that $p(z|x)$

equal to $q_\varphi(z|x)$, the ELBO is tight. The final objective of VAEs is the average over the data distribution:

$$\mathcal{L}_{ELBO}(x; \theta, \varphi) = \mathbb{E}_{p_D(x)}[\mathcal{L}_{ELBO}] \leq \mathbb{E}_{p_D(x)}[\log p_\theta(x)]. \quad (4)$$

The above knowledge can support the patch-wise distribution modelling and the theoretical derivation in Section D.

Hilbert-Schmidt Independence Criterion. Mutual information (MI) for representation learning has a long history. MI measures the amount of information one can obtain from one random variable given another [50]. The MI between two variables X and Y can be stated formally as

$$I(X; Y) = H(X) - H(X|Y) = H(Y) - H(Y|X), \quad (5)$$

which can also be estimated with the KL divergence:

$$\begin{aligned} I(X; Z) &= D_{KL}(p(x, z) \parallel p(x)p(z)), \\ &= \mathbb{E}_{p(x, z)} \left[\log \frac{p(x, z)}{p(x)p(z)} \right]. \end{aligned} \quad (6)$$

However, calculating the mutual information is practically difficult since the joint distribution is always intractable. Like MI, Hilbert-Schmidt Independence Criterion (HSIC), proposed by [51], is an effective method for testing independence that $HSIC(X, Y) = 0$ if and only if X and Y are independent. The essence is that $\text{Cov}(s(X), t(Y)) = 0$ implies independence, where $s \in \mathcal{F}$ and $t \in \mathcal{G}$ are all bounded continuous functions on Reproducing Kernel Hilbert Spaces (RKHS). Unlike MI, HSIC is a kernel-based measure:

$$HSIC(X; Y) = \|C_{XY}\|_{HS}^2, \quad (7)$$

where $\|\cdot\|_{HS}$ denotes the Hilbert-Schmidt norm, C_{XY} is the cross-covariance operator between two variables. According to [51], the empirical estimation of HSIC is defined as:

$$\begin{aligned} \widehat{HSIC}(X; Y) &= \frac{1}{n^2} \text{tr}(\mathbf{K}_X \mathbf{H} \mathbf{K}_Y \mathbf{H}) \\ &= \frac{1}{n^2} \text{tr}(X X^T Y Y^T) = \frac{1}{n^2} \text{tr}\|X^T Y\|_{HS}^2, \end{aligned} \quad (8)$$

where \mathbf{K}_X and \mathbf{K}_Y are kernel Gram matrices of X and Y and $\mathbf{H} = \mathbf{I} - \frac{1}{n}\mathbf{1}\mathbf{1}^T$ is the centering matrix.

Wasserstein measure. We start with the definition of Wasserstein distance (WD), which is derived from the optimal transport theory and forms a measure function between two probability distributions:

$$W_p(p_X, p_Y) = \inf_{\gamma \in \Pi(p_X, p_Y)} \mathbb{E}_{(X, Y) \sim \gamma} [d^p(X, Y)]^{\frac{1}{p}}, \quad (9)$$

where X, Y are random variables (e.g., features) whose marginal distributions are p_X and p_Y respectively and $\Pi(p_X, p_Y)$ means the set of all joint distributions (i.e., transport maps), d is a metric function. Note that in a majority of computer science and engineering studies, $d^p(x, y) = |x - y|^p$ is the Euclidean distance. Here W_p , refers to as the p -Wasserstein distance. When $p = 1$, the Kantorovich-Rubinstein duality is

$$W_1(p_X, p_Y) = \sup_{f \in \text{Lip}^1} \mathbb{E}_{X \sim p_X} [f(X)] - \mathbb{E}_{Y \sim p_Y} [f(Y)], \quad (10)$$

where Lip^1 is the family of all 1-Lipschitz functions. In the case of autoencoder, a relaxed version of the primal W_p is used for optimization, the details can be seen in [25]. These provide the distribution measure in Section E.

C. Patch-wise Distribution Modelling

As we pointed out before, robustly conducting anomaly screening based on existing generative methods on high-dimensional data is challenging. One main reason is that the posterior distribution of variational inference is intractable [13]. Therefore, researchers introduce the amortized latent distribution then approximate it to a given prior distribution $p(z)$. This latent distribution is expected to be informative and easy to be optimized. However, the common prior distribution (e.g. Gaussian distribution $\mathcal{N}(\mu, \sigma^2)$) with restricted stochastic process chiefly impedes the development of variational generative models. It is naturally to consider a mixture model prior, like Gaussian mixture models ($\sum_i \phi_i \mathcal{N}(\mu_i, \sigma_i^2)$), to increase the expressive capability of the latent distribution[21][22], yet the KL term in (Eq. 3) cannot be computed in the closed form.

In addition, we notice that there is plenty of works modelling image manifold via different patch characteristic then inspecting on each patch to check whether there exists a defect [17][23][24]. For example, Wang et al. [17] propose Local-Net to learn the feature of patch and Global-Net to extract context information from the surroundings, respectively. However, there is an impediment to applying these research works to real-world applications that the patches sampling mechanism, and equally the sufficient expressiveness is not explicitly courted. Meanwhile, one mentionable work in unsupervised representation learning community is *jigsaw puzzle* [32]. Given the shuffled image tiles as inputs, and trains the network to re-order them. This encourages the learned features to identify each tile in an object and how parts are constituted. Thus, we resort to whether can learn patch-wise statistics to increase the generative capability of the latent prior distribution with such a method.

In this paper, we propose a patch-wise variational autoencoder coupling with solving *jigsaw puzzle* to alleviate the contradiction between the simply and mixture prior distribution,

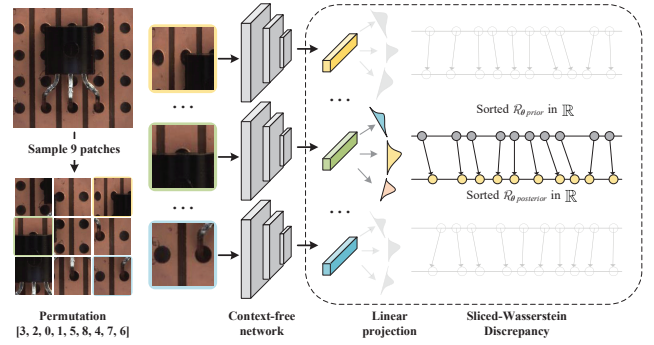


Fig. 3: The implementation variational inference patches using the context-free network. We introduce sliced-Wasserstein discrepancy to measure two distributions, which can avoid reparameterizing. (The similar operations are set transparent)

as shown in Fig. 2. It is a simple yet neat approach that converts the approximating mixture model prior distributions into a closed form prior optimization. In particular, we start by separate the training images using a regular $n \times n$ grid of patches $x = \{x^1, \dots, x^k, \dots, x^{n^2}\}$. Then the patches are shuffled according to the pseudo-label of permutation S_i . Following [32], the context-free network (CFN) is employed to extract features and inference tiles, as Fig. 3 shows. This is beneficial to eliminate the correlation of low-level features among each patch for ordering. Specially, based on the n^2 Siamese-wise encoder $f_\varphi(\cdot)$, the amortized inference posterior distribution of each tile $q(z^k|x^k)$ is got. Following the variational inference philosophy, the objective is to minimize the difference between the $q(z^k|x^k)$ and the prior $p(z^k)$.

It is natural that taking Gaussian distribution as each prior $p(z^k) = \mathcal{N}(\mu^k, \sigma^{k^2})$, however, empirical evidence shows that the normal training data boundary is sensitive to the noise, which has a further effect on the few seen instances. In other words, some patterns encoded at the tail biases the distribution. In this paper, for improving the robustness of inference distribution, we introduce the Student's t-distribution $\mathcal{T}(\nu, \mu, \sigma^2)$ [50] as the prior $p(z^k)$ for the latent features of each grid x^k :

$$p(z^k) = \mathcal{T}(z^k) = \frac{\Gamma(\frac{\nu^k+1}{2})}{\sqrt{\nu^k} \pi \Gamma(\frac{\nu^k}{2})} \left(1 + \frac{z^{k^2}}{\nu^k}\right)^{-\frac{\nu^k+1}{2}}, \quad (11)$$

where Γ is the gamma function and ν denotes the number of degrees of freedom. These can be set differently according to each patch. In the end, the accumulated patch inference distribution $\sum q(z^k|x^k)$ could be approximated according to their mixture of Student's t-distribution priors $\sum \mathcal{T}(z^k)$, respectively. However, the Student's t-distribution does not allow simply closed-form optimization in KL divergence (Eq. 3). In the Section 3. E, we will provide how to utilize sliced-Wasserstein to measure the divergence.

D. Hilbert-Schmidt Independence Criterion Bottleneck

In this part, we will elaborate on the implementation of the HSIC bottleneck in autoencoder for anomaly detection. Before introducing the core, we will illustrate the relationship

between the mutual information (**Eq. 6**) and the ELBO (**Eq. 4**), which can provide us a heuristic understanding of the variational inference from the information theory point of view. As shown in the preliminary, when $p(z|x) = q_\varphi(z|x)$, the objective (ELBO in **Eq. 3**) is tight. In this case, minimizing the KL divergence between $q_\varphi(z|x)$ and a prior $p(z)$ makes contributions to maximizing the ELBO:

$$D_{KL}(q_\varphi(z|x) \parallel p(z)) = \mathbb{E}_{p_D(x)} \left[q_\varphi(z|x) \log \frac{q_\varphi(z|x)}{p(z)} \right]. \quad (12)$$

In particular, this is achieved by the reparameterizing trick [13]. However, merely minimizing the KL divergence would induce generative network $f_\theta(\cdot)$ ignoring the latent variables of the inputs, as a consequence, the reconstruction is uninformative [25]. Here, we will demonstrate this problem from the mutual information perspective.

Firstly, the variational upper bound on mutual information is provided. Upper bounding MI is difficult, but not for estimation, we only use it to illustrate the relationship. Likewise, with introducing an amortized variational approximation $q_\varphi(z|x)$, a tractable variational upper bound [47] can be get by the Bayes' rule and multiplying and dividing the by $q_\varphi(z|x)$ on **Eq. 6**:

$$\begin{aligned} I(X; Z) &= \mathbb{E}_{p(x,z)} \left[\log \frac{p(x,z)}{p(x)p(z)} \right] \\ &= \mathbb{E}_{p(x,z)} \left[\log \frac{p(z|x)}{p(z)} \right] \\ &= \mathbb{E}_{p(x,z)} \left[\log \frac{q_\varphi(z|x)p(z|x)}{p(z)q_\varphi(z|x)} \right] \\ &= \mathbb{E}_{p(x,z)} \left[\log \frac{p(z|x)}{q_\varphi(z|x)} \right] - \mathbb{E}_{p(x,z)} \left[\log \frac{p(z)}{q_\varphi(z|x)} \right] \\ &= \mathbb{E}_{p_D(x)} \left[D_{KL}(p(z|x) \parallel q_\varphi(z|x)) \right] \\ &\quad - D_{KL}(p(z) \parallel q_\varphi(z|x)) \\ &\geq \mathbb{E}_{p_D(x)} \left[D_{KL}(p(z|x) \parallel q_\varphi(z|x)) \right]. \end{aligned} \quad (13)$$

So minimizing the KL divergence between the true posterior distribution $p(z|x)$ and the amortized distribution $q_\varphi(z|x)$ has the same effect on minimizing the upper bound on MI of the latent representation and its input $I(X; Z)$, over the average of the training normal dataset $p_D(x)$. If and only if the amortized inference distribution $q_\varphi(z|x)$ equals to the given prior distribution $p(z)$, the upper bound is tight. In this case, the $\mathbb{E}_{p_D(x)}[D_{KL}(p(z|x) \parallel q_\varphi(z|x))]$ equals to the mutual information between X and Z . Recall the objective of variational autoencoder (ELBO in **Eq. 3**), which turns to minimize the discrepancy between $q_\varphi(z|x)$ and $p(z)$ (even if the $D_{KL}(p(z) \parallel q_\varphi(z|x)) \neq D_{KL}(q_\varphi(z|x) \parallel p(z))$) under the assumption that the $p(z|x) = q_\varphi(z|x)$. Interestingly, the well approximated variational autoencoder will present zero mutual information with the same assumption.

Here, we show the contradiction between the ELBO and the MI. This can be understood the explanation of the first problem in InfoVAE [43] that the ELBO favors fitting the data distribution over performing correct inference. This makes the approximate inference distribution $q_\varphi(z|x)$ is different from the true posterior $p(z|x)$, which further may overfit the uninformative prior distribution. [43] proposes a mutual

information-based objective to weigh the preference between correct inference and approximating data distribution. Moreover, the information bottleneck (IB) [27] is optimized to constrain the entropy of latent features about inputs and outputs [19]. Since the complex computation of the mutual information in practical applications, the IB-based variational inference for AD is hard to develop.

In this paper, we explore a novel objective for variational autoencoder-based AD to mitigate the above problem and balance the inference and the representation. Specially, we introduce the Hilbert-Schmidt independence criterion (HSIC) [51][28], a non-parametric kernel-based method, to estimate the statistical dependence of the latent variables and the inputs. Similar with other statistical tests (e.g. t -test), given two random variables X and Z , the HSIC test is used to distinguish the null hypothesis $\mathcal{H}_0 : P_{XZ} = P_X P_Z$, and the alternative hypothesis $\mathcal{H}_1 : P_{XZ} \neq P_X P_Z$. The HSIC is widely used feature selection [51], robust representation learning [28]. However, there are few works that adopt the HSIC in variational autoencoder, especially in anomaly detection.

With the trade-off between the distribution approximation and true data representation in the mind, we utilize the HSIC to measure the (in)dependence of the accumulated patches latent variable $Z \in \mathbb{R}^{m \times n}$ and the prior distribution random variable $Z' \in \mathbb{R}^{m \times n}$ HSIC($Z'; Z$), and the input variables $X \in \mathbb{R}^{m \times d}$ HSIC($X; Z$), respectively. Here, m denotes the mini-batch size, d, n is the dimension of the input and latent features, individually. Following the work [28], the normalized cross-covariance is used in the normalized HSIC (nHSIC) which can be formulated by extending **Eq. 8**:

$$\text{nHSIC}(X, Z) = \text{tr}(\tilde{\mathbf{K}}_X \tilde{\mathbf{K}}_Z), \quad (14)$$

where $\tilde{\mathbf{K}}_X = \bar{\mathbf{K}}_X (\bar{\mathbf{K}}_X + \epsilon m \mathbf{I}_m)^{-1}$, likewise $\tilde{\mathbf{K}}_Z$. $\bar{\mathbf{K}}_X$ is centered of kernel matrices ($\mathbf{K}_X \in \mathbb{R}^{m \times m}$), and ϵ is a disturbance. According to **Eq. 8**, the \mathbf{K}_X has the entries $\mathbf{K}_{X_{ij}} = k(x_i, x_j)$, likewise \mathbf{K}_Z . In this paper, the kernel choice is the Gaussian kernel $k(x_i, x_j) \sim \exp(-\frac{1}{2} \|x_i - x_j\|^2 / \sigma^2)$. Implementing the IB [27] principle, the final HSIC bottleneck objective can be formulated as:

$$\mathcal{L}_{HSIC} = \text{nHSIC}(Z', Z) - \beta \text{nHSIC}(X, Z), \quad (15)$$

where the β denotes the trade-off between the dependence with the true data distribution and the prior distribution. Different from the previous works [27][28] minimizing the dependence between the latent variable and the input, our proposed HSIC bottleneck is to maximize it, since the (pseudo)label in the variational inference is the true data distribution. Based on the theoretical demonstration of the contradiction between the ELBO and the MI, our proposed optimization function can mitigate the conflict between the approximation inference distribution and fitting the data distribution.

E. P-WAE Framework for Anomaly Detection

In this part, we will summarize the above contributions and provide the framework of our proposed P-WAE for anomaly detection. Retrospecting the one-class classification-based AD, the core is to learn a parameterized network that modelling the

Algorithm 1: Optimization flow of P-WAE framework for AD

Require: Learning a generalized network for modelling the normal data distribution $p_D(x)$;

Procedure:

Initialize networks $f_\varphi(\cdot)$, $f_\theta(\cdot)$, $h_j(\cdot)$;

while not converged **do**

- 1: Randomly sample from the normal dataset: $x_i \sim p_D(x)$;
- 2: Separate and shuffle patches according to the pseudo-label $x_i = \{x_i^1, \dots, x_i^k, \dots, x_i^{n^2}\} \sim S_i$;
- 3: Inference the latent posterior distribution of each patch: $q_\varphi(z^k|x^k) = f_\varphi(x_i^k)$;
- 4: Calculate the SWD between the inference distribution and the prior distribution of each patch with Eq. 18: \mathcal{L}_{SWD} ;
- 5: Calculate the HSIC between the input variable X and the accumulated latent codes Z : $\text{nHSIC}(X, Z)$;
- 6: Calculate the HSIC between Z' and Z : $\text{nHSIC}(Z', Z)$, $\mathcal{L}_{HSIC} = \text{nHSIC}(Z', Z) - \beta \text{nHSIC}(X, Z)$;
- 7: Solve the *jigsaw puzzle* with Z : \mathcal{L}_{jigsaw} ;
- 8: Generate (reconstruct) the data: $\hat{x} = f_\varphi(f_\theta(x))$;
- 9: Calculate the reconstruction error: $\mathcal{L}_{AE} = \|\hat{x} - x\|_n$;
- 10: Δ Updates $f_\varphi(\cdot)$ with \mathcal{L}_{SWD} and \mathcal{L}_{HSIC} ;
- 11: Δ Updates $f_\varphi(\cdot)$, $h_j(\cdot)$ with \mathcal{L}_{jigsaw} ;
- 12: Δ Updates $f_\varphi(\cdot)$, $f_\theta(\cdot)$ with \mathcal{L}_{AE} ;

end while

normal data distribution, while the anomaly can be detected as out-of-distribution cases. Such a parameterized network can be the P-WAE architecture. As shown in Fig. 1, the whole network includes two main part: (1) a context-free inference network $f_\varphi(\cdot)$; (2) jigsaw generative network $f_\theta(\cdot)$. Given normal instances x_i from the true normal distributing $p_D(X)$, we first shuffle the image tiles according to the pseudo-permutation label S_i . Each patch is sent to $f_\varphi(\cdot)$, then the latent features z_i is approximated. As we discussed before, the KL divergence is a strong distance notation and has related shortcomings for approximation. Meanwhile, it does not allow the closed form of the Student's t-distribution $\mathcal{T}(\nu, \mu, \sigma^2)$. Therefore, in this paper, we introduce the sliced-Wasserstein distance [22] to measure the distributions, as shown in Fig. 3.

Extended by **Eq. 10**, but the Sliced-Wasserstein distance (SWD) can alleviate its high computational cost via linear slicing (Radon transform) the probability distribution:

$$\mathcal{R}_{p_X}(t; \vartheta) = \int_X p_X(x) \delta(t - \vartheta \cdot x) dx, \forall \vartheta \in \mathbb{S}^{d-1}, \forall t \in \mathbb{R}, \quad (16)$$

where \mathbb{S}^{d-1} stands for the d-dimensional unit sphere and $\delta(\cdot)$ denotes the one-dimensional Dirac delta function. For a fixed ϑ , $\mathcal{R}_{p_X}(\cdot; \vartheta)$ is a marginal distribution of p_X . Based on it, the sliced-Wasserstein distance used for distribution difference measure between the prior distribution $p(z^k)$ and the inference posterior $q(z^k|x^k)$ could be defined as:

$$SW_p(p(z^k), q(z^k|x^k)) = \left(\int_{\mathbb{S}^{d-1}} W_p(\mathcal{R}_{p(z^k)}(\cdot; \vartheta), \mathcal{R}_{q(z^k|x^k)}(\cdot; \vartheta)) d\vartheta \right)^{\frac{1}{p}}. \quad (17)$$

In particular, the accumulated inference loss function is the

sum of each patch's sliced-Wasserstein distance:

$$\begin{aligned} \mathcal{L}_{SWD} &= \sum_k^{n^2} SW_p(p(z^k), q(z^k|x^k)) \\ &\approx \sum_k^{n^2} \frac{1}{|\Theta|^k} \sum_{\vartheta \in \Theta^k} W_p(\mathcal{R}_{p(z^k)}(\cdot; \vartheta), \mathcal{R}_{q(z^k|x^k)}(\cdot; \vartheta)), \end{aligned} \quad (18)$$

where Θ^k denotes a finite set of the d-dimensional unit sphere \mathbb{S}^{d-1} , n^2 is the number of the patches. This could technically replace the KL divergence in the variational autoencoder.

In addition, after approximation, the latent codes of all patches are assembled then dedicated to permutation recognition. This auxiliary task (i.e. solving *jigsaw puzzle*) encourages the network to learn the structural information, which endows the network with both local and global perception. Taken overall, we jointly train the parameters of the inference network $f_\varphi(\cdot)$ and the permutation classification network $h_j(\cdot)$ though minimizing the cross-entropy:

$$\mathcal{L}_{jigsaw} = - \sum_i^N p(S_i) \log p(\hat{S}_i | z^1, \dots, z^k, \dots, z^{n^2}). \quad (19)$$

In conclusion, during the training phase, given the defect-free instances, the objective function involves four parts:

$$\mathcal{L} = \mathcal{L}_{AE} + \lambda_1 \mathcal{L}_{HSIC} + \lambda_2 \mathcal{L}_{SWD} + \lambda_3 \mathcal{L}_{jigsaw}, \quad (20)$$

where λ_1 , λ_2 and λ_3 are hyperparameters, \mathcal{L}_{AE} can be the mean squared error (MSE) between the input data and the reconstructed one ($\sum_i \|y_i - x_i\|^2$), \mathcal{L}_{HSIC} denotes the HSIC bottleneck for collapsed representations (Eq. 15), \mathcal{L}_{SWD} is the inference distribution loss (Eq. 18), and \mathcal{L}_{jigsaw} represents the permutation classification error (Eq. 19). The process can be seen on the Algorithm 1 table. With these, the network is to model the true normal distribution, with facility. During the testing stage, the algebraic sum of the entire image and each patch tile reconstruction error are estimated to screen the anomaly. The criterion for the defect-free instances is that both the reconstruction error of the whole image and each patch should be lower than the threshold, and vice versa:

$$\|x_i, \hat{x}_i\|_2 \leq \epsilon_0 \in \mathbb{R} \wedge \|x_i^k, \hat{x}_i^k\|_2 \leq \epsilon_k \in \mathbb{R}. \quad (21)$$

IV. EXPERIMENT

A. Experiment Setup

Datasets: To demonstrate the superior performance and generalization ability of our proposed P-WAE model, experiments are conducted on a recent real-world benchmark – MVTEC AD [2]. The dataset includes 5,354 high-resolution industrial images which are divided into 5 textures and 10 objects categories. The training dataset contains 3,629 normal images, and the labeled test set consists of 1,725 defect-free (non-anomalous) or abnormal instances. This configures an unsupervised anomaly detection scenario that only provides normal samples during training. Details of MVTEC AD are reported in [2]. In this paper, we follow the original dataset split (i.e. only training on the normal and test on both).

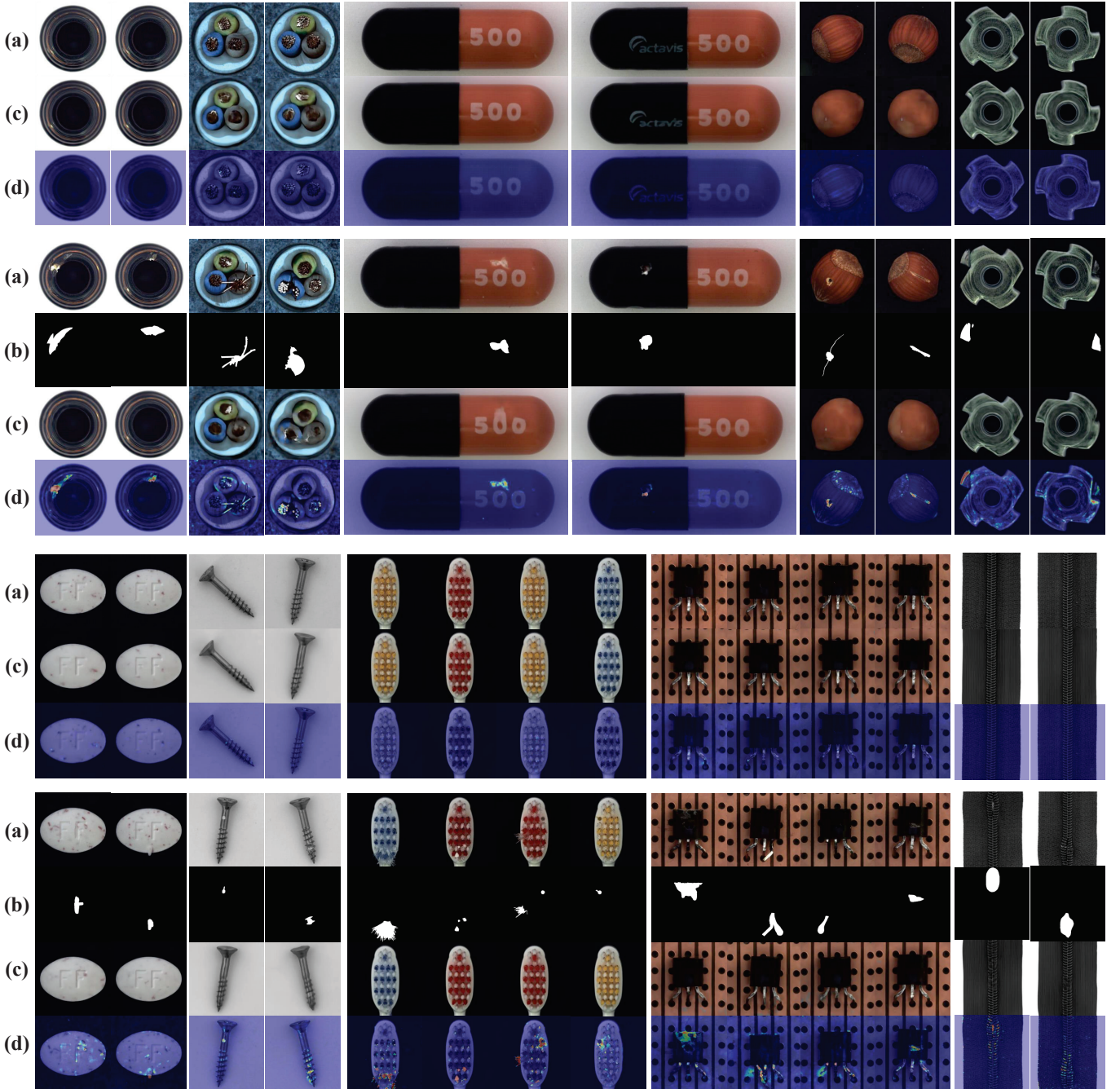


Fig. 4: The visualization of the anomaly detection results. (a) the input images; (b) the anomaly region mask; (c) the reconstruction; (d) the difference between the reconstruction and the input.

Implementation details: Given a normal sample during training, the first two are defining the grid size ($n \times n$) to separate the image as patches and the cardinality of the patch permutation subset S . Following [32], we keep the $n = 3$, and S contains 1000 random permutations. That is we split an image into 9 patches, and for each training iteration, the patches are sent to the Siamese-network $f_\varphi(\cdot)$, in parallel. The inference network $f_\varphi(\cdot)$ is implemented with a standard pre-trained ResNet-50 network on ImageNet [52]. Removing the final fully-connected layer, we frame the penultimate layer as the latent feature mapper h_p . For each patch latent feature

z_i^k , we assign the Student's t-distribution $\mathcal{T}(5, k, 1)$ as the prior distribution, where 5 is the degree of freedom. The reason for utilizing the degree of 5 is that it is a trade-off between robustness and convergence. If the degree of freedom is too large, the t-distribution is similar to the bell curve. The separated latent features are then combined before reassembling by the flow-based warp. The generative network $f_\theta(\cdot)$ is built by multiple blocks which consist of Upsample-Conv-BN-ReLU layers. The auxiliary *jigsaw puzzle* classification head

h_j includes one fully-connected layer.¹

We resize the image to 300×300 and processed in 100×100 for one patch, except with the capsule category, whose images are resized to 1008×300 and processed in 336×100 for one patch. The hyper-parameter β in Eq. 15 is set as 0.1, and λ_1 , λ_2 , λ_3 in Eq. 20 is 0.01, 0.1, and 1, respectively. The stochastic gradient descent (SGD) with an initial learning rate (lr) of 0.01 and a momentum parameter of 0.9 is used to train the network. The learning rate is decayed with $lr = \frac{lr_0}{(1+ap)^b}$, where lr_0 is the initial learning rate and p linearly increases from zero to one. In our case, $a = 10$ and $b = 0.75$. All experiments based on Pytorch are deployed on NVIDIA GeForce GTX 3080 GPU and Intel Core i9-10900k CPU.

B. Results

Visualization results: Firstly, we visualize the reconstruction result and the reconstruction error for each category in Fig. 4. For each object, the top line is the result of defect-free instances, while the bottom line denotes the results of abnormal samples. It is obvious that the reconstruction is high-fidelity. And the error of normal samples is tiny while the abnormal region can be used to classify with high reconstruction error. Because it has to be reconstructed with its 'normal' version. In other word, with our proposed model, the anomaly region can be restored. Moreover, our proposed P-WAE has the capability to generate high-resolution data without blurry, and the comparison with existing methods is also shown in Fig. 1. Secondly, the visualization of learned representations distribution of each patch are shown by t-SNE [53] in Fig. 5. As expected, the latent distribution of each defect-free (good) samples patch clusters together while the abnormal patches do not follow it. This is the requisite ability for AD network, which encourage to detect and localize the anomaly region. The visualization of those latent distributions is further proof of the interpretability of our proposed patch-wise modelling method. It is observed from the figure that the representations of anomaly patches are often entanglement with others. Finally, we show that the smooth latent space of trained P-WAE in Fig. 6. The linear interpolations in the z -space demonstrate that (i) our proposed model is able to map real images into the latent space and generate it back; (ii) the diverse query input data can be found in this smooth z -space. This is vital for preventing the collapsed model.

Numerical results: With the reconstruction-based anomaly detection philosophy, we also take the reconstruction error as the criterion to classify. Like previous work [40], the reconstruction error can be defined as l_2 distance between the input x_i and the reconstruction image \hat{x}_i :

$$Error_i = \|x_i, \hat{x}_i\|_2 \leq \epsilon_0 \in \mathbb{R}. \quad (22)$$

When the $Error_i$ less than the threshold ϵ_0 , it can be classified as normal sample. Unlike previous work, we additionally consider the patch reconstruction error:

$$Error_i^k = \|x_i^k, \hat{x}_i^k\|_2 \leq \epsilon_k \in \mathbb{R}. \quad (23)$$

Based on this, the anomaly detection criterion is that if all the whole image reconstruction error $Error_i$ and each patch reconstruction error $Error_i^k$ are less than the threshold, the instance can be classified as a defect-free sample. On the other hand, if there is one patch reconstruction error $Error_i^k$ or the whole image error $Error_i$ beyond the threshold, it should be detected as an anomaly. After normalizing, the error and the threshold are from 0 to 1.

To quantitatively analyze the quality of the proposed approach, we introduce two evaluation metrics. Following the work [44], the Maximum Balanced Accuracy and the Area Under the ROC Curve (AUROC) are utilized. The first one denotes the mean of the true positive rate (TPR) and true negative rate (TNR). In our case, the TPR is the ratio of correctly classified anomalies and TNR represents the ratio of correctly classified defect-free data. The AUROC is used as a threshold-independent quality metric for classification. We report and compare those metrics per category.

The comparison between our proposed network (P-WAE) and several state-of-the-art anomaly detection methods on MVTEC AD dataset is provided. In particular, these methods include iterative-based algorithms, such as AnoGAN [3], γ -VAE_g [15], VQ-VAE [18]; single-pass-based techniques, such as SSIM-AE [40] and l_2 -AE [40], EGBAD [41], LSA [38], GeoTrans [36], GANomaly [42], ITAE [37], and CBiGAN [44]. Moreover, the CAVGA [16] is compared even it adopts additional data. The results for each methods and for each category are indicated in Table I and II. Compared with VQ-VAE-based AD [15], which also utilizes the variational inference, we can see that our model consistently improves the detection of anomalies in a lot of categories by at most 30% (with Cable), achieving a +4% improvement on the average Maximum Balanced Accuracy. It is reported that compared with adversarial-based network, such as AnoGAN [3] and CBiGAN [44], our proposed P-WAE achieves superior performance, especially for object categories, such as improving by at most 62% (with Screw), 43% (with Cable). A similar conclusion can be observed from the AUROC metric. Compared with the state-of-the-art methods, such as ITAE [37] – a data augmentation-based autoencoder, P-WAE maintains or improves the detection performance in most categories by at most 32% (with Capsule), achieving a +3% improvement on the average AUROC.

Both metrics prove that P-WAE improves on all the compared algorithms, reaching respectively an average Mean Balanced Accuracy and AUROC of 0.89 and 0.87 without additional data. Considering all categories, our method outperforms the existing method from 34% to 4% (with Mean Balanced Accuracy), and from 27% to 3% (with AUROC). In addition, Fig. 1 shows the comparison between the reconstruction of the previous work and P-WAE. Note that due to the vanilla autoencoder does not consider the distribution, the reconstruction is easy to be biased toward the anomaly input. And the variational autoencoder is hampered by the over-smooth problem. While our P-WAE reports high-resolution virtual reconstructions.

¹Code is available: <https://github.com/YurongChen1998/yurong-lib>

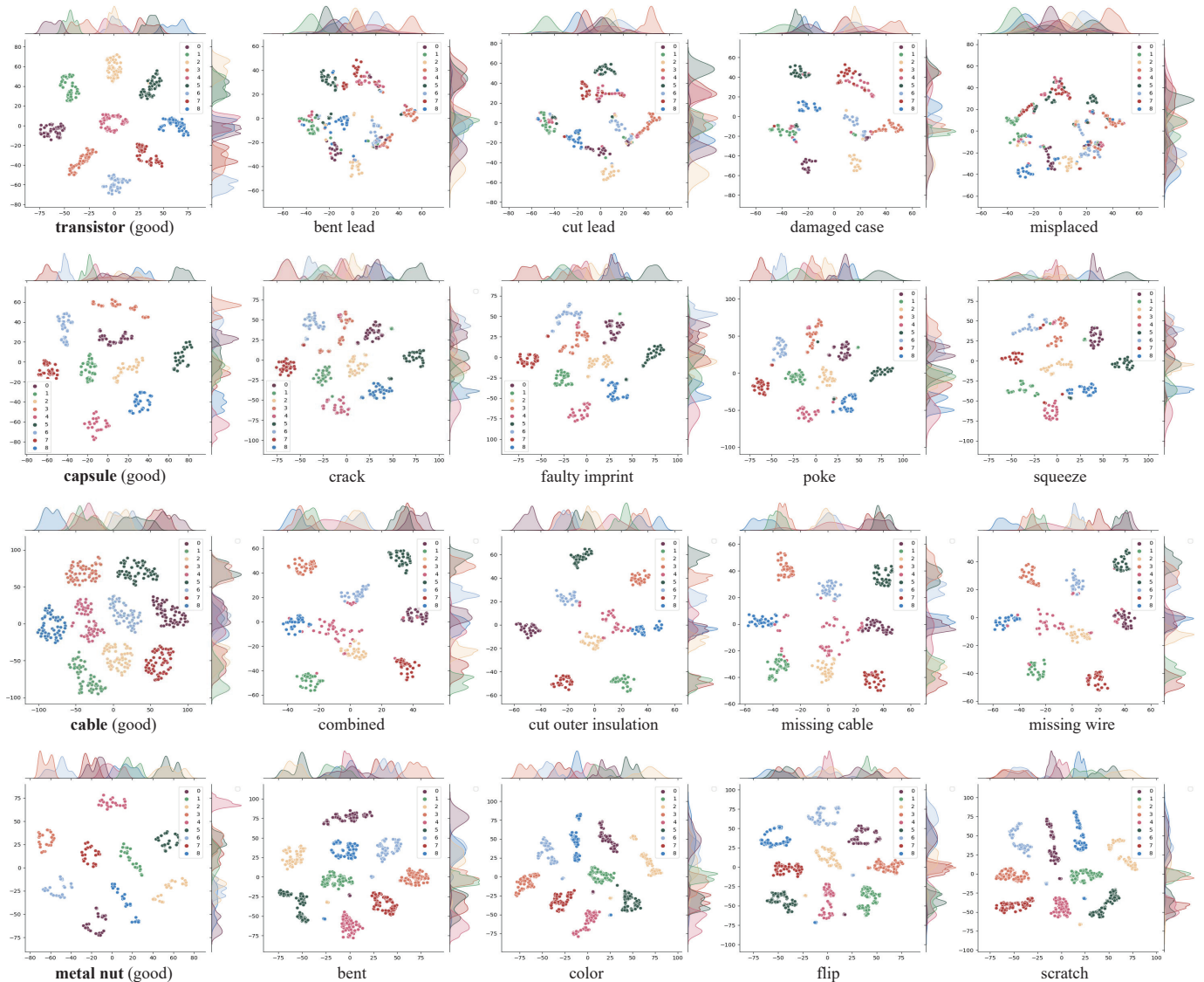


Fig. 5: T-SNE visualization of latent distribution for defect-free (the first row) and anomalies. We split each image into nine patches as the experiment setting. The first row shows that each tile clusters together without outlier, while there are deviations in other rows. Compared with whole image inference-based methods, our proposed method is more prone to localize anomalies.

C. Ablation Experiments

Effect of the HSIC: We conduct experiments on testing the feature diversity of trained models. As we discussed before, one main difficulty for applying previous variational inference-based methods [13][19] in the real-world scenarios is the collapsed feature. This adverse phenomenon challenges the model generalization on unseen datasets. In this paper, we propose P-WAE to alleviate this problem. We compare the feature diversity of Deep autoencoder (AE) [29], variational autoencoder (VAE) [13], our proposed P-WAE without HSIC bottleneck objective, and the complete P-WAE network (with HSIC). We visualize the probability density function of normalized latent feature z on a 2-dim space with a Gaussian kernel density estimation (KDE) which with bandwidth estimated by Scott's Rule [54]. Darker areas denote more concentrated features [55]. The results can be seen in Fig. 7 that we observe the

feature diversity of AE and VAE is highly linear dependent. While P-WAE without HSIC (the third column) can generate diverse features, the HSIC (the last column) has a significantly beneficial effect on feature independence.

V. CONCLUSION

In this paper, we propose a generalized one-class anomaly detection method, Patch-wise Wasserstein AutoEncoder (P-WAE). Based on the variational inference framework, we learn the model to fit the normal data distribution, while the anomaly can be detected as the out-of-distribution samples. In particular, we mitigate the two problems of this framework in anomaly detection: (i) the limited prior distribution; (ii) the collapsed feature. Therefore, the robustness and generalization of the model are improved that applying to reality becomes likely. Compared with the-state-of-art algorithms, extensive

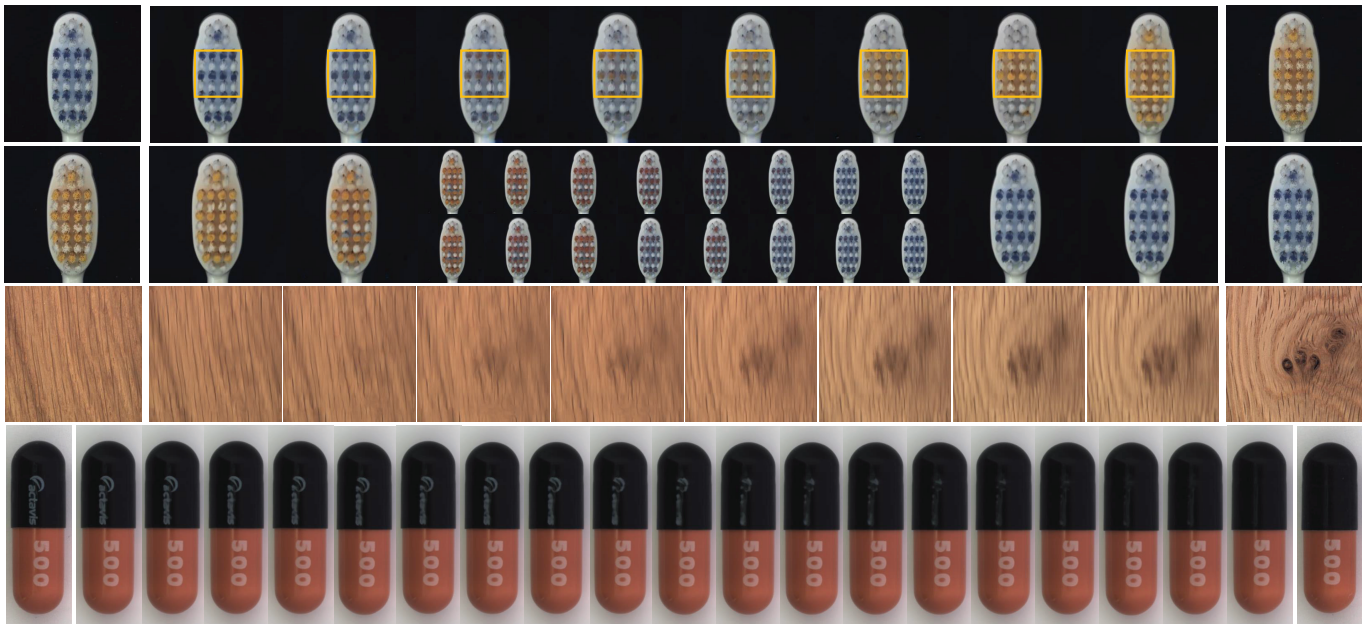


Fig. 6: Interpolations in the latent space of the trained P-WAE. The first row indicates that only linear interpolation in one patch latent space. The last three rows are linear interpolations in the whole image latent space. Those interpolations are operated between two latent codes conditioned by real image inputs (the first and last column).

TABLE I: Comparison results among different anomaly detection methods in the anomaly detection task on MVTEC AD for each category. Maximum Balanced Accuracy $B = (\text{TPR} + \text{TNR})/2$ is utilized as the evaluation metric.

Category	AnoGAN [3]	EGBAD [41]	SSIM-AE [40]	l_2 -AE [40]	LSA [38]	CBiGAN [44]	$\gamma - VAE_g$ [15]	CAVGA - D_u [16]	CAVGA - R_u [16]	VQ-VAE [18]	P-WAE (Ours)
Carpet	0.49	0.60	0.67	0.50	0.74	0.60	0.67	0.73	0.78	0.71	0.69
Grid	0.51	0.50	0.69	0.78	0.54	0.99	0.83	0.75	0.78	0.91	0.88
Leather	0.52	0.65	0.46	0.44	0.70	0.87	0.71	0.71	0.75	0.96	0.93
Tile	0.51	0.73	0.52	0.77	0.70	0.84	0.81	0.70	0.72	0.95	0.89
Wood	0.68	0.80	0.83	0.74	0.75	0.88	0.89	0.85	0.88	0.96	0.96
Bottle	0.69	0.68	0.88	0.80	0.86	0.84	0.86	0.89	0.91	0.99	0.99
Cable	0.53	0.66	0.61	0.56	0.61	0.73	0.56	0.63	0.67	0.72	0.96
Capsule	0.58	0.55	0.61	0.62	0.71	0.58	0.86	0.83	0.87	0.68	0.98
Hazelnut	0.50	0.50	0.54	0.88	0.80	0.75	0.74	0.84	0.87	0.94	0.84
Metal Nut	0.50	0.55	0.54	0.73	0.67	0.67	0.78	0.67	0.71	0.83	0.76
Pill	0.62	0.63	0.60	0.62	0.85	0.76	0.80	0.88	0.91	0.68	0.73
Screw	0.35	0.50	0.51	0.69	0.75	0.67	0.71	0.77	0.78	0.80	0.97
Toothbrush	0.57	0.48	0.74	0.98	0.89	0.97	0.89	0.91	0.97	0.92	1.00
Transistor	0.67	0.68	0.52	0.71	0.50	0.74	0.70	0.73	0.75	0.73	0.78
Zipper	0.59	0.59	0.80	0.80	0.88	0.55	0.67	0.87	0.94	0.97	0.92
Avg.	0.55	0.61	0.63	0.71	0.73	0.76	0.77	0.78	0.82	0.85	0.89

experimental results on a real-world benchmark (i.e. MVTEC AD) demonstrate the validity of our method.

REFERENCES

- [1] P. Stern, "Perception of dangerous animals," *Science*, vol. 352, no. 6290, pp. 1186-1187, 2016.
- [2] P. Bergmann, M. Fauser, D. Sattlegger, and C. Steger, "MVTEC AD – A comprehensive real-world dataset for unsupervised anomaly detection," in *Computer Vision and Pattern Recognition (CVPR)*, 2019.
- [3] T. Schlegl, P. Seeböck, S. Waldstein, et al., "Unsupervised anomaly detection with generative adversarial networks to guide marker discovery," in *IPMI*, 2017.
- [4] T. Xiang and S. Gong, "Video behavior profiling for anomaly detection," in *IEEE Transactions on Pattern Analysis and Machine Intelligence*, vol. 30, no. 5, pp. 893-908, 2008.
- [5] F. Edgeworth, "On discordant observations," *Philosophical Magazine*, vol. 23, no. 5, pp. 364–375, 1887.
- [6] C. Varun, A. Banerjee, and V. Kumar, "Anomaly detection: A survey," *ACM computing surveys*, vol.41, no.3, pp. 1-58, 2009
- [7] M. Sabokrou, M. Fayyaz, M. Fathy and R. Klette, "Deep-cascade: Cascading 3D deep neural networks for fast anomaly detection and localization in crowded scenes," in *IEEE Transactions on Image Processing*, vol. 26, no. 4, pp. 1992-2004, 2017.
- [8] K. Cheng, Y. Chen and W. Fang, "Gaussian process regression-based video anomaly detection and localization with hierarchical feature representation," in *IEEE Transactions on Image Processing*, vol. 24, no. 12, pp. 5288-5301, 2015.
- [9] X. Zhou, Y. Wang, Q. Zhu.; J. Mao, C. Xiao, X. Lu, and H. Zhang, "A surface defect detection framework for glass bottle bottom using visual attention model and wavelet transform," in *IEEE Transactions on Industrial Informatics*, vol. 16, no. 4, pp. 2189-2201, 2020.
- [10] P. Perera and V. M. Patel, "Learning deep features for one-class classification," *IEEE Transactions on Image Processing*, vol. 28, no. 11, pp. 5450-5463, 2019.
- [11] L. Ruff, R. Vandermeulen, N. Goernitz, et al., "Deep one-class classifi-

TABLE II: Comparison results among different anomaly detection methods in the image-level anomaly detection task on MVtec AD. Area Under the ROC curve (AUROC) is utilized as the evaluation metric.

Category	EGBAD [41]	GeoTrans [36]	l_2 -AE [40]	GANomaly [42]	CBiGAN [44]	ITAE [37]	P-WAE (Ours)
Carpet	0.52	0.44	0.64	0.70	0.55	0.71	0.70
Grid	0.54	0.62	0.83	0.71	0.99	0.88	0.90
Leather	0.55	0.84	0.80	0.84	0.83	0.86	0.81
Tile	0.79	0.42	0.74	0.79	0.91	0.74	0.87
Wood	0.91	0.61	0.97	0.83	0.95	0.92	0.92
Bottle	0.63	0.74	0.65	0.89	0.97	0.94	0.99
Cable	0.68	0.78	0.64	0.76	0.81	0.83	0.93
Capsule	0.52	0.67	0.62	0.73	0.56	0.68	1.00
Hazelnut	0.43	0.36	0.73	0.79	0.77	0.86	0.76
Metal Nut	0.47	0.81	0.64	0.70	0.63	0.67	0.86
Pill	0.57	0.63	0.77	0.74	0.81	0.79	0.83
Screw	0.46	0.50	1.00	0.75	0.58	1.00	0.92
Toothbrush	0.64	0.97	0.77	0.65	0.94	1.00	1.00
Transistor	0.73	0.87	0.65	0.79	0.77	0.84	0.76
Zipper	0.58	0.82	0.87	0.75	0.53	0.88	0.80
Avg.	0.60	0.67	0.75	0.76	0.77	0.84	0.87

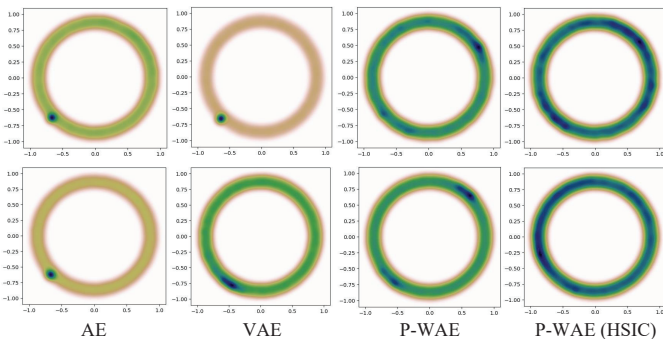


Fig. 7: Feature diversity on MVtec AD (bottle category) images in \mathbb{R}^2 with Gaussian kernel density estimation (KDE). Darker areas indicate more concentrated features that the feature diversity is limited.

- cation,” in *International Conference on Machine Learning (ICML)*, 2018, pp. 4393-4402.
- [12] B. Scholkopf, J. Platt, J. Shawe-Taylor, A. Smola, and R. Williamson, ”Estimating the support of a high dimensional distribution,” *Neural computation*, vol. 13, no. 7, pp. 1443-1471, 2001.
- [13] D. P. Kingma, and M. Welling, ”Auto-Encoding variational Bayes,” in *International Conference on Machine Learning (ICML)*, 2014.
- [14] I. Goodfellow, J. Pouget-Abadie, M. Mirza, B. Xu, D. Warde-Farley, S. Ozair, A. Courville, and Y. Bengio, ”Generative adversarial nets,” in *Conference on Neural Information Processing Systems (NeurIPS)*, 2014, pp. 2672-2680.
- [15] D. Dehaene, O. Frigo, S. Combexelle, and P. Eline, ”Iterative energy-based projection on a normal data manifold for anomaly localization,” in *International Conference on Learning Representation (ICLR)*, 2020.
- [16] S. Venkataramanan, K. Peng, R. Singh, and A. Mahalanobis, ”Attention guided anomaly detection and localization in images,” in *European Conference on Computer Vision (ECCV)*, 2019.
- [17] S. Wang, L. Wu, L. Cui, and Y. Shen, ”Glancing at the patch: anomaly localization with global and local feature comparison,” in *Computer Vision and Pattern Recognition (CVPR)*, 2021, pp. 254-263.
- [18] L. Wang, D. Zhang, J. Guo, Y. Han, ”Image anomaly detection using normal data only by latent space resampling,” *Applied Sciences*, vol. 10, no. 23, pp. 8660, 2020.
- [19] A. Alemi, I. Fischer, J. Dillon, and K. Murphy, ”Deep variational information bottleneck,” in *International Conference on Learning Representation (ICLR)*, 2017.
- [20] L. Mescheder, S. Nowozin, A. Geiger, ”Adversarial variational bayes: Unifying variational autoencoders and generative adversarial networks,” in *International Conference on Machine Learning (ICML)*, 2017, pp. 2391-2400.
- [21] B. Zong, Q. Song, M. Min, et al., ”Deep autoencoding Gaussian mixture model for unsupervised anomaly detection,” in *International Conference on Learning Representation (ICLR)*, 2018.
- [22] S. Kolouri, G. Rohde, H. Hoffmann, ”Sliced wasserstein distance for learning Gaussian mixture models,” in *Computer Vision and Pattern Recognition (CVPR)*, 2018: 3427-3436.
- [23] J. Yi, S. Yoon, ”Patch SVDD: Patch-level SVDD for anomaly detection and segmentation,” in *Asian Conference on Computer Vision (ACCV)*, 2020.
- [24] D. Carrera, F. Manganini, G. Boracchi and E. Lanzarone, ”Defect detection in SEM images of nanofibrous materials,” in *IEEE Transactions on Industrial Informatics*, vol. 13, no. 2, pp. 551-561, 2017.
- [25] I. Tolstikhin, O. Bousquet, S. Gelly, et al., ”Wasserstein auto-encoders,” in *International Conference on Learning Representation (ICLR)*, 2018.
- [26] J. Lucas, G. Tucker, R. Grosse, et al., ”Don’t blame the ELBO! A linear VAE perspective on posterior collapse,” in *Conference on Neural Information Processing Systems (NeurIPS)*, 2019.
- [27] N. Tishby, and N. Zaslavsky, ”Deep learning and the information bottleneck principle,” in *IEEE Information Theory Workshop*, 2015, pp. 1-5.
- [28] W. Ma, J. Lewis, W. Kleijn, ”The HSIC bottleneck: Deep learning without back-propagation,” in *the AAAI Conference on Artificial Intelligence*, 2020, pp. 5085-5092.
- [29] G. Hinton, and R. Salakhutdinov, ”Reducing the dimensionality of data with neural networks,” *Science*, vol. 313, no. 5786, pp. 504-507, 2006.
- [30] Y. Yang, Q. M. J. Wu and Y. Wang, ”Autoencoder with invertible functions for dimension reduction and image reconstruction,” in *IEEE Transactions on Systems, Man, and Cybernetics: Systems*, vol. 48, no. 7, pp. 1065-1079, 2018.
- [31] A. N. Paul, P. Yan, Y. Yang, H. Zhang, S. Du and Q. M. Jonathan Wu, ”Non-iterative online sequential learning strategy for autoencoder and classifier,” *Neural Computing and Applications*, 2021.
- [32] M. Noroozi, P. Favaro, ”Unsupervised learning of visual representations by solving jigsaw puzzles,” in *European Conference on Computer Vision (ECCV)*, 2016, pp. 69-84.
- [33] V. Barnett and T. Lewis, *Outliers in statistical data*, 1994.
- [34] D. Tax and R. Duin. ”Support vector data description,” *Machine Learning* vol. 54, no. 1, pp. 45-66, 2004.
- [35] P. Perera and V. M. Patel, ”Learning deep features for one-class classification,” in *IEEE Transactions on Image Processing*, vol. 28, no. 11, pp. 5450-5463, 2019.
- [36] I. Golan and R. ElYaniv, ”Deep anomaly detection using geometric transformations,” in *Conference on Neural Information Processing Systems (NeurIPS)*, 2018.
- [37] C. Huang, J. Cao, F. Ye, M. Li, Y. Zhang, and C. Lu, ”Inverse-transform autoencoder for anomaly detection,” *arXiv preprint arXiv:1911.10676*, 2019.
- [38] D. Abati, A. Porrello, S. Calderara, and R. Cucchiara, ”Latent space autoregression for novelty detection,” in *Computer Vision and Pattern Recognition (CVPR)*, 2019, pp. 481-490.
- [39] Z. Wang, A. C. Bovik, H. R. Sheikh, and E. P. Simoncelli, ”Image quality assessment: from error visibility to structural similarity,” in *IEEE Transactions on Image Processing*, vol. 13, no. 4, pp. 600-612, 2004.
- [40] P. Bergmann, S. Lowe, M. Fauser, D. Sattlegger, and C. Steger, ”Improving unsupervised defect segmentation by applying structural similarity to autoencoders,” in *International Joint Conference on Computer Vision, Imaging and Computer Graphics Theory and Applications (VISAPP)*, 2019, pp. 372-380.
- [41] H. Zenati, C. Foo, B. Lecouat, G. Manek, and V. Chandrasekhar, ”Efficient gan-based anomaly detection,” in *International Conference on Learning Representation Workshop (ICLRW)*, 2018.
- [42] S. Akcay, A. Atapour-Abarghouei, and T. P. Breckon, ”GANomaly: Semi-supervised anomaly detection via adversarial training,” in *Asian Conference on Computer Vision (ACCV)*, 2018.
- [43] S. Zhao, J. Song, S. Ermon, ”Infovae: Balancing learning and inference in variational autoencoders,” in *the AAAI Conference on Artificial Intelligence*, 2019, pp. 5885-5892.
- [44] F. Carrara, G. Amato, L. Brombin, F. Falchi and C. Gennaro, ”Combining GANs and AutoEncoders for efficient anomaly detection,” in *International Conference on Pattern Recognition (ICPR)*, 2021, pp. 3939-3946.
- [45] J. Goldberger, S. Gordon and H. Greenspan, ”Unsupervised image-set clustering using an information theoretic framework,” in *IEEE Transactions on Image Processing*, vol. 15, no. 2, pp. 449-458, 2006.

- [46] R. Linsker, "Self-organization in a perceptual network," *Computer*, vol. 21, no. 3, pp. 105-117, 1988.
- [47] B. Poole, S. Ozair, A. Oord, et al., "On variational bounds of mutual information," in *International Conference on Machine Learning (ICML)*, 2019, pp. 5171-5180.
- [48] D. Barber, and F. Agakov, "The im algorithm: A variational approach to information maximization," in *Conference on Neural Information Processing Systems (NeurIPS)*, 2003, pp. 201-208.
- [49] A. Alemi, B. Poole, I. Fischer, et al., "Fixing a broken ELBO," in *International Conference on Machine Learning (ICML)*, 2018.
- [50] K.P. Murphy, *Machine learning: a probabilistic perspective*, 2012.
- [51] A. Gretton, K. Fukumizu, C. Teo, L. Song, B. Schölkopf, and A. Smola, "A kernel statistical test of independence," in *Conference on Neural Information Processing Systems (NeurIPS)*, 2007, pp. 585-592.
- [52] J. Deng, W. Dong, R. Socher, L. Li, K. Li, and L. Fei-Fei, "Imagenet: A large-scale hierarchical image database," in *Computer Vision and Pattern Recognition (CVPR)*, 2009.
- [53] L. Maaten and G. Hinton, "Visualizing data using t-sne," *Journal of machine learning research*, vol. 9, pp. 2579-2605, 2008.
- [54] D. Scott, *Multivariate density estimation: theory, practice, and visualization*, John Wiley & Sons, 2015.
- [55] W. Chen, Z. Yu, S. Mello, S. Liu, M. Alvarez, Z. Wang, and A. Anandkumar, "Contrastive syn-to-real generalization," *International Conference on Learning Representation (ICLR)*, 2020.